Proceedings 10th NUMGE 2023
10th European Conference on Numerical Methods in Geotechnical Engineering
Zdravkovic L, Kontoe S, Taborda DMG, Tsiampousi A (eds)

https://doi.org/10.53243/NUMGE2023-9

Finite element modelling of earth pressure on integral bridge piles

M. D'Ignazio[1,2] , V. Lehtonen[1], L. P. Savolainen[1], P. Tolla[3], V.-M. Uotinen[3]

[1]*Ramboll Finland Oy, Finland*
[2]*Department of Civil Engineering, Tampere University, Tampere, Finland*
[3]*Finnish Transport Infrastructure Agency (FTIA), Finland*

ABSTRACT: In Finland, integral bridges are often founded on piles, especially in presence of difficult soil conditions, which often consist of very soft and highly compressible soil. Structural design of piles for integral bridges is strongly affected by the earth pressure acting along the piles during the construction of the road embankment and superstructure and under the action of traffic loads. The mobilized earth pressure is commonly determined analytically based on a simplified solution according to a national design code. This solution models the earth pressure increment based on the earth pressure coefficient at rest of the embankment/superstructure material and assuming a given stress distribution with depth. Soil conditions and drainage during loading are expected to have an impact on the actual earth pressure. These aspects cannot be captured by the simplified analytical solution. Therefore, this study aims to compare the existing analytical approach to 3D finite element analyses. Finally, an improved analytical solution is proposed based on the finite element results.

Keywords: earth pressure; bridge; pile; analytical solution; 3D FEA

1 INTRODUCTION

In Finland, pile foundations are commonly adopted to support integral bridges. This is due to the presence of very soft and highly compressible soils. The earth pressure mobilized under the operational traffic loads will highly impact the structural design of piles.

In Finland, bridge designers model the mobilized earth pressure on piles using an analytical solution described in Tiehallinto (2007). This solution accounts for the weight of the soil above the pile and the applied traffic load. The resulting earth pressure increment is calculated based on the earth pressure coefficient at rest (K_0) of the embankment/superstructure material and assuming a 2:1 stress distribution with depth. In practice, the earth pressure is also affected by soil conditions and drainage characteristics. The analytical solution does not account for such features of soil.

The aim of this study is to compare the existing analytical approach for modelling earth pressure on integral bridge piles to 3D Finite Element analyses carried out with the FE software PLAXIS 3D by Bentley. Analyses are carried out for two integral bridge configurations with two piles with 5 m spacing and for two subsoil types: a medium dense to dense sand and a clay. A 5 m-high embankment with additional 3 m-high superstructure with 10 m top width is considered. Two embankment configurations are modelled assuming crushed rock and sand materials. The surface loads considered are the road traffic loads according to NCCI 7 for Eurocode 7 (Liikennevirasto, 2017) and train loads according to Liikennevirasto (2018). Finally, an improved analytical solution is proposed based on the FE results.

The study has been funded by the FTIA. This paper summarizes the results that are presented in detail in FTIA (2020).

2 ANALYTICAL SOLUTION FOR EARTH PRESSURE ON INTEGRAL BRIDGE PILES

Figure 1 shows the Tiehallinto (2007) analytical solution for earth pressure increments acting on bridge abutment piles. The solution considers the unit weight (γ) and the earth pressure coefficient at rest (K_0) of the embankment/superstructure material located above the pile heads, over a height H. Further, it accounts for the effects of traffic loads (P). Being z the vertical coordinate, the earth pressure increment at $z=H$ induced by the superstructure ($P1$) and the traffic load ($P2$) are:

$$P1 = \gamma \cdot H \cdot K_0 \quad (1)$$

$$P1' = P1 \cdot B/(B + z) \quad (2)$$

$$P2 = P \cdot K_0 \quad (3)$$

$$P2' = P2 \cdot B/(B + z) \quad (4)$$

Where B is the top width of the superstructure. The earth pressure distribution along the piles is calculated following a 2:1 load distribution with depth and according to B. Further, the solution assumes that the earth pressure is "gathered" from a 3-pile-diameter width, meaning that the analytical curves should be multiplied by a factor of three; and that the earth pressure increment is negligible below a depth of $1.2h$ from the top of the superstructure, where h is the thickness of the embankment + superstructure.

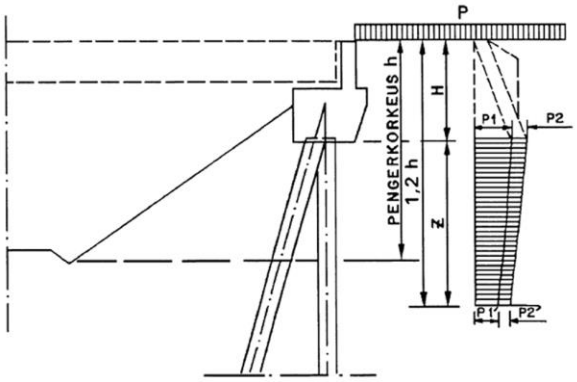

Figure 1. Analytical solution for earth pressure increments on bridge piles – Adapted from Tiehallinto (2007), where "pengerkorkeus" indicates the height of embankment + superstructure.

3 PROBLEM FRAMEWORK

3.1 Geometry

Figure 2 shows the reference geometries used in this study for two bridge configurations:

- Integral bridge with cantilever span (hereinafter referred to as Cantilever or **CA**) and n.2 piles with diameter D=0.813 m and 5 m spacing
- Integral bridge without cantilever span (hereinafter referred to as Non-Cantilever or **NCA**) and n.2 piles with diameter D=0.813 m and 5 m spacing

A 5 m-thick embankment with 3 m-thick road pavement or track super and substructure is considered on top of an 8 m-thick subsoil (sand or clay) resting over a 3 m-thick moraine layer. The embankment slope is 1:1.5 for crushed rock and 1:2 for sand embankment. The groundwater table (GWT) is set 1.5 m below the subsoil surface. N.2 piles with D=0.813 m are modelled with a 5 m spacing. The piles are 15 m (NCA) and 17 m (CA) long with 2 m embedment in the deep moraine layer.

The pile head is modelled as fully fixed in the NCA case. Fully fixed and fully free pile head conditions are analysed for the CA case. The reason is that these would describe different scenarios of bearing on top of the pile. In practice, the bearing on top of the pile should not be modelled as a spring, but rather assuming a constant friction. In any case, the friction is relatively low already in the case of a new bearing (friction coefficient ≈0.06), and it reduces to almost zero for an old bearing (≈0.002). Given that friction forces are negligible compared to the expected earth pressures, the pile head is modelled as both fully free and fully fixed to evaluate the effect of pile head fixity on the behaviour.

The loads are applied 2 m from the abutment wall (as a way of simplifying the effect of the transition slab). The distance between the pile centreline and the abutment wall is 0.6 m and 2 m for the NCA and CA layouts, respectively.

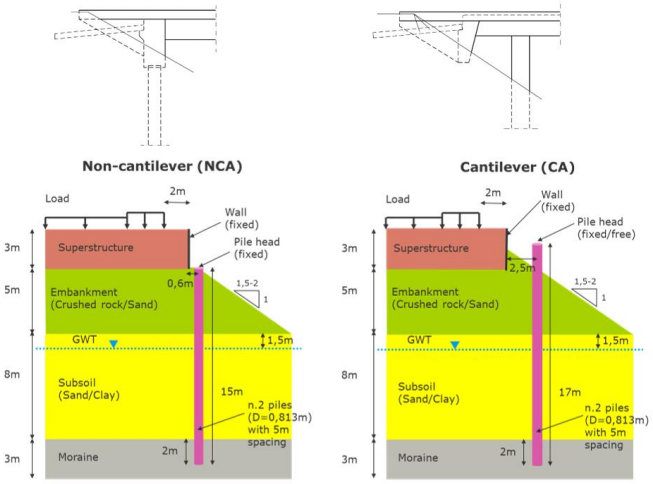

Figure 2. Schematization of NCA and CA bridge abutments with piles used in this study (not in scale).

3.2 Loads

The loads considered in this study are:

- Traffic loads: 9 kPa distributed, 9+31 (3x5 m) kPa - NCCI 7 (Liikennevirasto, 2017)
- Train LM-71 max load: 52 (3x6.4 m) kPa + 27 kPa (3 m width); 52 (3x6.4 m) load on bogies – repeated at 6.1 m distance (Rato 3, Liikennevirasto, 2018)

3.3 Calculation matrix

The calculation matrix presented in Figure 3 summarizes all the different calculations that are carried out. A progressive number and an ID are assigned to each calculation, according to the following nomenclature:

Bridge type - Embankment material - Subsoil & Pile-head fixity - Load type

Legend:
Bridge type: **CA** for cantilever; **NCA** for non-cantilever
Embankment material: **01** for crushed rock with 1:1.5 slope; **02** for sand with 1:2 slope
Subsoil: **S** for sand; **C** for clay
Pile-head fixity: **1** for fully fixed; **2** for fully-free
Load type: **T** for traffic load (9 + 31 kPa); **R1** for distributed 52 kPa+27 kPa LM-71 load; **R2** for 52 kPa LM-71 load on bogies

Bridge type	Embankment	Subsoil	Pile-head fixity	Load	ID	N.
Cantilever	Crushed rock	Sand	Fixed	9+31 kPa	CA-01-S1-T	1
				LM-71 v1	CA-01-S1-R1	2
				LM-71 v2	CA-01-S1-R2	3
			Free	9+31 kPa	CA-01-S2-T	4
				LM-71 v1	CA-01-S2-R1	5
				LM-71 v2	CA-01-S2-R2	6
		Clay	Fixed	9+31 kPa	CA-01-C1-T	7
				LM-71 v1	CA-01-C1-R1	8
				LM-71 v2	CA-01-C1-R2	9
			Free	9+31 kPa	CA-01-C2-T	10
				LM-71 v1	CA-01-C2-R1	11
				LM-71 v2	CA-01-C2-R2	12
	Sand	Sand	Fixed	9+31 kPa	CA-02-S1-T	13
				LM-71 v1	CA-02-S1-R1	14
				LM-71 v2	CA-02-S1-R2	15
			Free	9+31 kPa	CA-02-S2-T	16
				LM-71 v1	CA-02-S2-R1	17
				LM-71 v2	CA-02-S2-R2	18
		Clay	Fixed	9+31 kPa	CA-02-C1-T	19
				LM-71 v1	CA-02-C1-R1	20
				LM-71 v2	CA-02-C1-R2	21
			Free	9+31 kPa	CA-02-C2-T	22
				LM-71 v1	CA-02-C2-R1	23
				LM-71 v2	CA-02-C2-R2	24
Non-Cantilever	Crushed rock	Sand	Fixed	9+31 kPa	NCA-01-S1-T	25
				LM-71 v1	NCA-01-S1-R1	26
				LM-71 v2	NCA-01-S1-R2	27
		Clay	Fixed	9+31 kPa	NCA-01-C1-T	28
				LM-71 v1	NCA-01-C1-R1	29
				LM-71 v2	NCA-01-C1-R2	30
	Sand	Sand	Fixed	9+31 kPa	NCA-02-S1-T	31
				LM-71 v1	NCA-02-S1-R1	32
				LM-71 v2	NCA-02-S1-R2	33
		Clay	Fixed	9+31 kPa	NCA-02-C1-T	34
				LM-71 v1	NCA-02-C1-R1	35
				LM-71 v2	NCA-02-C1-R1	36

Legend	
Crushed rock	01
Sand	02
Sand	S
Clay	C
Fixed	1
Free	2
Traffic	T
Railway	R
Distributed	1
Bogies	2

Figure 3. Calculation matrix.

4 FINITE ELEMENT MODEL

4.1 Geometry and construction phases

Figures 4 and 5 show the PLAXIS 3D FE geometries for CA and NCA bridge configurations, respectively, including soil layering and all the elements, model dimensions and FE mesh. The soil volumes are modelled with 10-noded tetrahedral elements, and the mesh consist of around 35 000 elements. Despite the model symmetry along the y-axis, the full model was required for the analyses because of the non-symmetric traffic load applied. Interface elements are modelled around the piles.

The initial stresses in the subsoil are generated through a "K_0 phase", where the soil weight is applied, and stresses are defined according to K_0. The 5 m embankment is modelled as a drained material and applied by gravity in a plastic calculation phase. In a subsequent phase, piles are activated. Later, the 3 m superstructure and loads are applied. Firstly, the 3 m superstructure, modelled as drained, is applied and the earth pressure mobilized. Secondly, additional earth pressure mobilization occurs under the applied load.

4.2 Earth pressure modelling

The earth pressure along the piles is modelled as the average stress acting on a surface right behind the pile. The surface width is taken equal to the pile diameter D=0.813 m. The reference surface is normal to the maximum displacement direction, which is inclined by an angle α from the x-direction. The concept is illustrated in Figure 6.

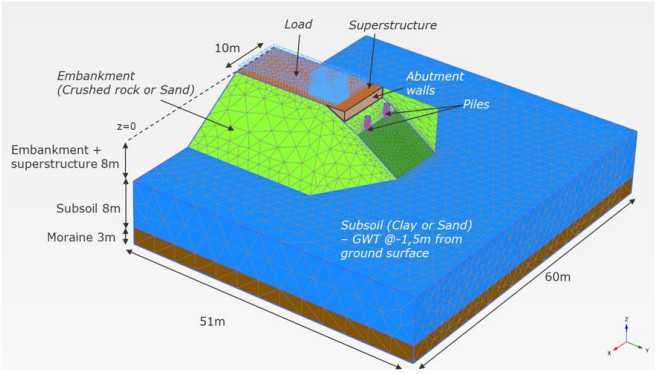

Figure 4. FE geometry and mesh – Cantilever (CA) model.

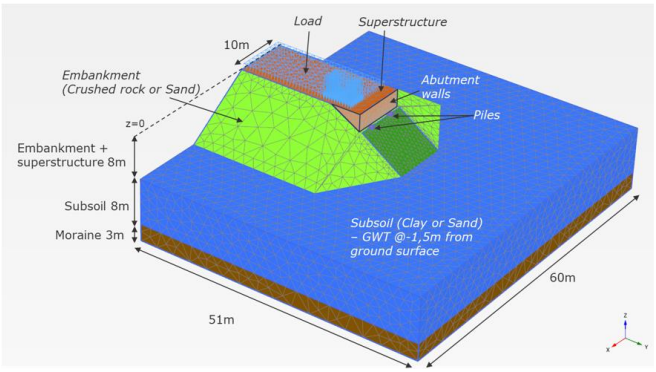

Figure 5. FE geometry and mesh – Non-Cantilever (NCA) model.

In general, α ranges between 10 and 15° for all the calculations. For α=10-15°, $\sigma_{max,\alpha}=\sigma_{normal}/\cos\alpha=\sigma_{yy}/\cos\alpha\approx\sigma_{yy}$. Therefore, for simplicity, the stresses acting in the y-direction are taken to model earth pressure. For drained and undrained layers, σ'_{yy} (effective) and σ_{yy} (total) are used, respectively.

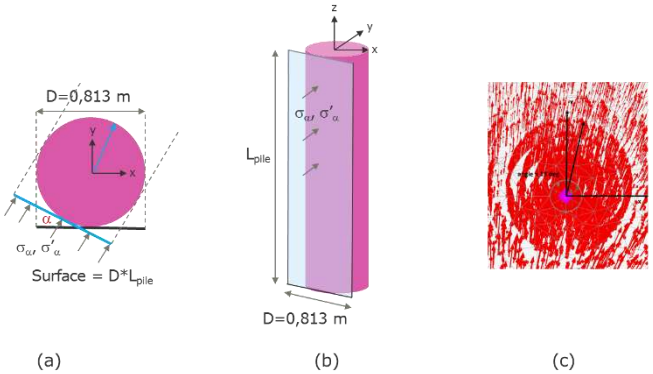

Figure 6. Selection of reference surface for modelling earth pressure acting along piles (a) top view and (b) 3D view. (c) Displacement vector under traffic load (CA-01-S1-T).

As shown in Figure 7, a large scatter characterizes the stress distribution across the surface. The scatter does not reduce significantly by improving the FE mesh around the pile. Hence, a moving average along the pile axis (z-axis) is calculated to define the average earth pressure acting along the pile.

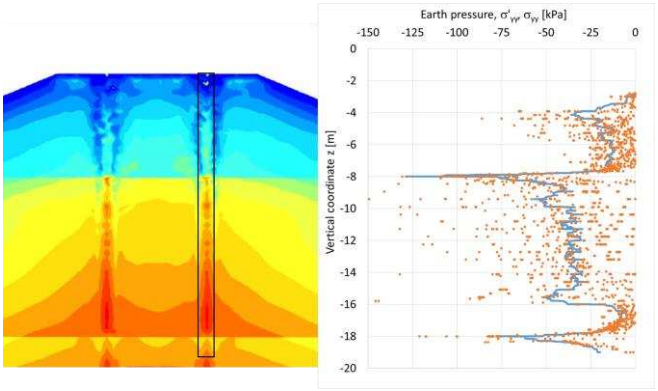

Figure 7. Illustration of cross-section used to model earth pressure and example of average earth pressure obtained for a point distribution across a surface with width equal to the pile diameter.

4.3 Material models and parameters

Coarse materials are modelled with the Hardening Soil model (Plaxis, 2020). These include the embankment, superstructure, sand subsoil and moraine. The Hardening Soil model is further used to simulate the long-term drained behaviour of the clay subsoil beneath the 5 m embankment, prior to construction of the superstructure and application of the loads. The undrained clay subsoil is otherwise modelled by the Tresca model, where the stiffness is selected so that it corresponds to fairy small strain levels. Tables 1 and 2 summarize the input parameters for Hardening Soil and Tresca models, respectively. A detailed description of model parameters can be found in Plaxis (2020).

Table 1. Input parameters for Hardening Soil model.

Parameter	Unit	Superstructure / Crushed rock / Sand / Moraine / Clay
$\gamma_{unsat} = \gamma_{sat}$	kN/m³	20 / 20 / 18 / 21 / 15.2
E_{50}^{ref}	MPa	160 / 120 / 50 / 120 / 0.9
E_{oed}^{ref}	MPa	135 / 110 / 55 / 110 / 0.9
E_{ur}^{ref}	MPa	320 / 360 / 150 / 360 / 18
c'	kPa	5 / 0.1 / 0.1 / 0.1 / 0.1
φ'	°	45 / 45 / 36 / 40 / 25
ψ	°	5 / 5 / 6 / 10 / 0
ν_{ur}	-	0.2
m	-	0.5 / 0.5 / 0.5 / 0.5 / 1
p^{ref}	kPa	100
K_0^{nc}	-	0.29 / 0.33 / 0.41 / 0.36 / 0.58
R_f	-	0.9
e	-	0.5 / 0.5 / 0.5 / 0.5 / 2
POP	kPa	0 / 0 / 0 / 0 / 20
R_{inter}	-	0.5 / 0.5 / 0.5 / 0.5 / 0.7
Drainage	-	Drained

The sand's friction angle ϕ'=36° and the clay's undrained shear strength s_u=40 kPa were given as an input by FTIA. The remaining model parameter were chosen as best estimate values based on literature and Authors' experience with Finnish soils.

Table 2. Input parameters for Tresca model.

Parameter	γ_{sat}	s_u	G/s_u	E_u/s_u	ν	R_{inter}
Unit	kN/m³	kPa	-	-	-	-
Clay	15.2	40	167	500	0.495	0.7

The piles are modelled as circular linear elastic volume elements with an elastic modulus E=42 GPa, Poisson's ratio ν=0.3, unit weight γ=28 kN/m³ and diameter D=0.813 m. The input parameters are calculated for composite reinforced concrete RR800/12.5 piles with steel grade S440J2H and bending stiffness EI≈900 MNm². For D=0.813 m, E≈42 GPa.

5 RESULTS

The traffic load produces a maximum settlement of ≈3-4 mm, as shown in the example of Figure 8. According to FTIA, this is in line with what is typically observed and somewhat validates the stiffness of the FE model. Further, displacements under the LM-71 loads are ≈4 mm for the case with sand subsoil and ≈6.5 mm for the case with clay subsoil. Similar values were found in all the NCA and CA cases analysed. The computed displacements were found to be substantially independent of the FE mesh used.

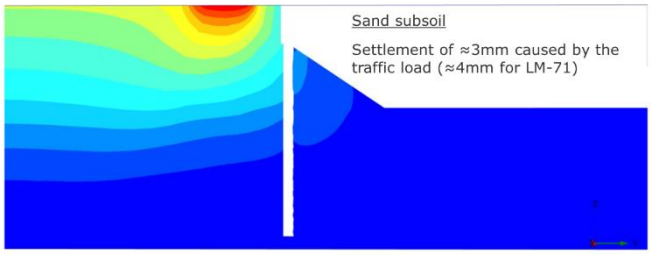

Figure 8. Vertical displacement under traffic load – longitudinal section @x=2,5m through the centreline of the pile – NCA-01-S1-T.

Figures 9 and 10 show comparison examples between the computed earth pressure under traffic and LM-71 loads and the analytical solutions for *P1* and *P2*. The analytical curves do not include the assumed multiplying factor of 3 that accounts for gathering of earth pressure from an area equal to 3 times the pile diameter. Since the two analysed LM-71 load configurations (distributed and bogies) give substantially similar results, only the "52 kPa + 27 kPa" LM-71 load results are presented together with the "9 kPa + 31 kPa" traffic load.

In the analytical solution for *P2*, average traffic/train loads are selected to model P and *P2* in equations (3) and (4). In detail, P = 10 kPa with B = 10 m and P = 32

kPa with B = 7.5 m are selected for traffic load and LM-71 load, respectively.

In most cases, the analytical solution appears to deviate from the FE results (FTIA, 2020). It severely underestimates the earth pressure in undrained conditions (Figure 10). The analytical solution seems to be more in line with the earth pressure in the coarse layers when the model is governed by drained conditions (i.e. sand subsoil). Nevertheless, the solution is based on K_0 conditions and it only accounts for the K_0 of the superstructure. On the other hand, the mobilized earth pressure may deviate from K_0 conditions according to the degree of mobilization.

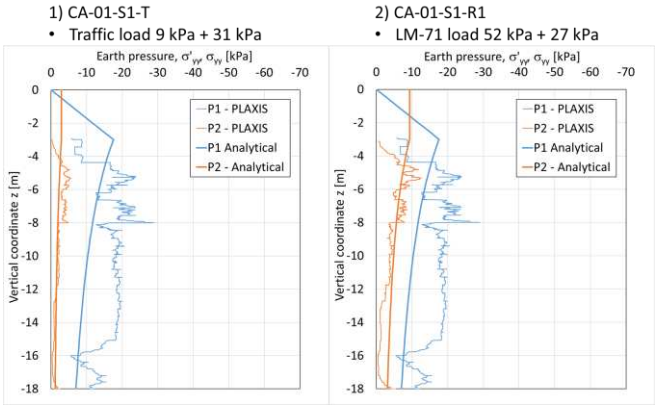

Figure 9. FE vs analytical earth pressure solution for CA-01-S1-T and CA-01-S1-R1 (embankment: crushed rock; subsoil: sand; pile head: fixed).

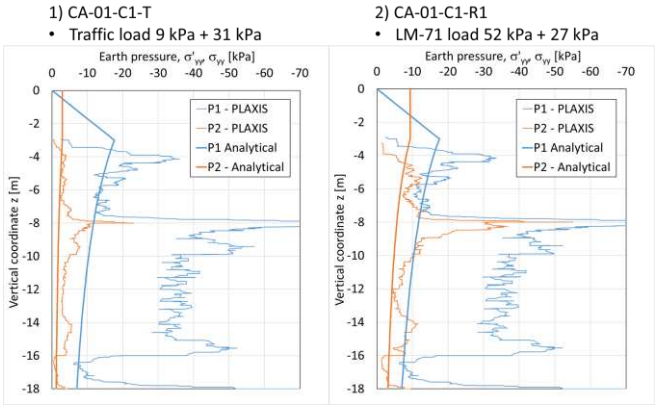

Figure 10. FE vs analytical earth pressure solution for CA-01-C1-T and CA-01-C1-R1 (embankment: crushed rock; subsoil: clay; pile head: fixed).

In undrained conditions, the two solutions deviate even in the coarse layers (Figure 10), especially for the NCA cases. One possible reason may be the high shear mobilization in the embankment that results from the simulation of long-term conditions (large settlement after construction). In this way, the embankment and superstructure will exhibit a softer behaviour compared to the case with sand subsoil, with consequent stress concentration and earth pressure increase behind the fixed piles. This behaviour seems to be less pronounced in the CA model with fixed pile head, while it tends to disappear when the pile head is free to move. It must be noted that the distance between the centre of the pile and the abutment wall is larger in the CA model (2.5 m) compared to the NCA model (0.6 m).

The computed horizontal pile displacement (u_y) from the combined superstructure and traffic load for the different NCA and CA models suggest u_y in clay approximately 5-6 times larger than in sand, with u_y generally lower than 8 mm. Overall, traffic (road or railway) loading seems to cause approximately 10% of the total pile movement when the pile head is modelled as fixed; while it causes approximately 15-20% of the total pile movement in the upper part of the pile with free head.

Furthermore, it was found that the earth pressure betwee the piles is lower than the average earth pressure acting along the piles. Similar distributions are obtained for clay subsoil and LM-71 train loads.

6 IMPROVED ANALYTICAL SOLUTION

An attempt to improve the current analytical solution based on FE results is presented here (Figure 11). A new set of equations for earth pressure increments *P1* and *P2* is proposed as follows:

$$P1\ (kPa) = \gamma \cdot H \cdot K_0 \qquad (5)$$

$$P1'(kPa) = \gamma \cdot H \cdot [B/(B+z)] \cdot K_0^i \cdot f \qquad (6)$$

$$P2\ (kPa) = q \cdot K_0 \qquad (7)$$

$$P2'(kPa) = q \cdot [B/(B+z)] \cdot K_0^i \cdot f \qquad (8)$$

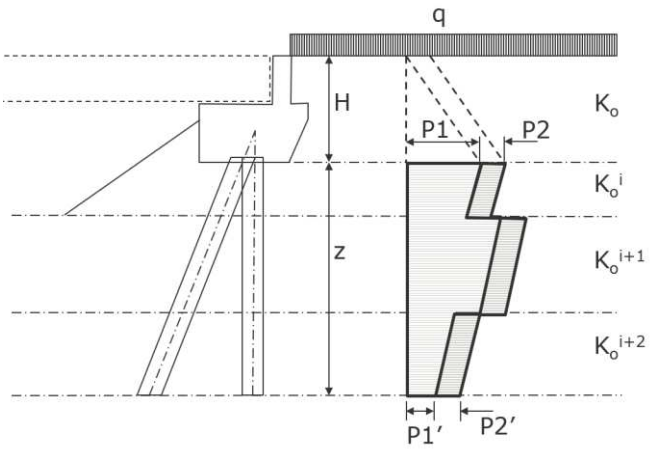

Figure 11. Illustration of improved analytical solution accounting for the variation of K_0 in each layer or with depth.

Compared to the 2007 solution, the traffic load symbol is changed from "*P*" to "*q*" for clarity. *B* is the width of the top of the embankment. The symbol *f* is a model factor. For each layer *i*, the vertical stress increment is multiplied by the layer-specific K_0^i value.

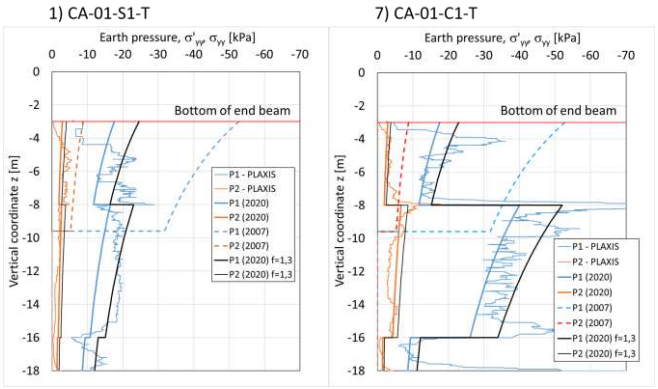

Figure 12. Comparison of calculation results and original (2007) and improved analytical solution for CA-01-S1-T and CA-01-C1-T (embankment: crushed rock; subsoil: sand/clay; pile head: fixed; road traffic load).

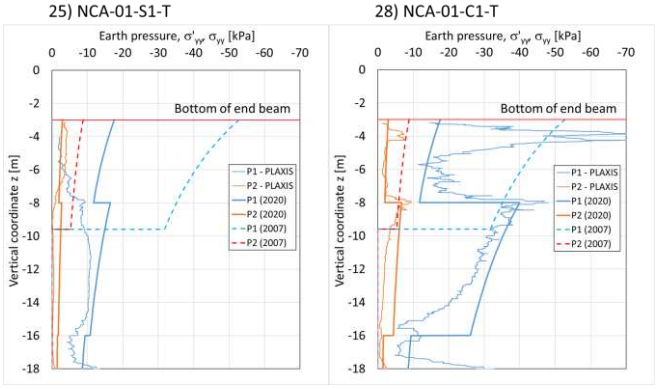

Figure 13. Comparison of calculation results and original (2007) and improved analytical solution for NCA-01-S1-T and NCA-01-C1-T (embankment: crushed rock; subsoil: sand/clay; pile head: fixed; road traffic load).

Figures 12 and 13 compare the computed and the analytical solutions for earth pressure. The 2007 curves account for the gathering effect of earth pressure over an area equal to 3 times the pile diameter. Therefore, a factor of 3 is applied to the basic curves, unlike in the previous section. The 2007 solution curves are cut here at 1.2h (embankment height with superstructure, h=8 m).

For the calculation of *P2*, a uniformly distributed road traffic load of q = 10 kPa was used. Unlike the original solution, the improved solution appears to be able to capture the earth pressure, especially in the undrained clay subsoil. The original solution overestimates the earth pressure in the drained layer above z=1.2h=-9.6m. Further, the FE results suggest that earth pressure develops below a depth of 1.2h. Therefore, it is not negligible as suggested by the current approach.

For the CA cases, a model factor f=1.3 appears to provide a reasonable fit to the computed earth pressure. For NCA, f=1 can be assumed. These model factors may change if pile spacing and geometry deviate from those considered in this study.

7 SUMMARY AND CONCLUSIONS

This study focused on earth pressure from traffic and train loads on integral bridge piles. The results of this study are exensively described in FTIA (2020). Two bridge configurations have been analysed: bridge with cantilever span (CA) and bridge without cantilever span (NCA). The main goal was to compare the analytical solution from Tiehallinto (2007) with the earth pressure from 3D Finite Element Analyses (FEA).

The scope of the FEA was to study the effect of using different bridge configurations, embankment materials and slope geometries, subsoils (clay, soft vs sand, stiff) and pile bearings (fully fixed vs free pile head) on the earth pressure under traffic and train loads.

Results show that in most cases the 2007 analytical solution deviates from the FE results, especially for undrained conditions, where it underestimates the earth pressure. The discrepancy is less evident for drained conditions. The analytical curves were not multiplied by a factor of 3 to account for the stress gathering effect behind the piles. This would have led to a severe overestimation of earth pressure, especially in the coarse layers. In the FEA, such a "gathering effect" for earth pressure was not visible. Moreover, earth pressure appears to develop over the entire pile length, in contrast with the recommendations given in previous guidelines.

An improved analytical solution was proposed based on the FEA. Unlike the standard solution, the improved solution can capture the earth pressure in the undrained layers. For the drained layers, the benefit is less evident. Model factors are proposed for CA and NCA bridge types. Moreover, the multiplying factor of 3 recommended in Tiehallinto (2007) appears to be conservative even when applied along with the improved solution. Note that these conclusions and proposed model factors are only valid for the pile spacing, geometry and construction phases adopted in this study.

8 REFERENCES

FTIA, 2020. Finite element modelling of earth pressure on abutment piles of integral bridges. Publication 32/2020, Finnish Transport Infrastructure Agency, Helsinki. Weblink: https://www.doria.fi/handle/10024/180089

Liikennevirasto. 2017. Eurokoodin soveltamisohje – Geotekninen suunnittelu NCCI 7. Siltojen ja pohjarakenteiden suunnitteluohjeet. Liikenneviraston ohjeita 13/2017.

Liikennevirasto. 2018. RATO 3. Ratatekniset ohjeet (RATO) osa 3. radan rakenne. Liikenneviraston ohjeita 13/2018.

PLAXIS, 2020. Bentley Plaxis user's manual.

Tiehallinto. 2007. Sillan geotekniset suunnitteluperusteet. Suunnitteluvaiheen ohjaus. Tiehallinto. Helsinki.